Published online: March 30, 2020

IMR Press

Original Research

Herbal complex '*Buyang Huanwu Tang*' improves motor endplate function of denervated-dependent skeletal muscle atrophy in rat

Lan Zhou[1], Yu-Fang Huang[2], Hui Xie[3], Xiao-Yun Mei[1,*] and Jun Cao[4,*]

[1]*Basic Theory of Traditional Chinese Medicine Staff Room, Basic Medical College, Nanjing University of Traditional Chinese Medicine, Nanjing, 210029, P. R. China*

[2]*Pathological Staff Room, Basic Medical College, Nanjing University of Traditional Chinese Medicine, Nanjing, 210029, P. R. China*

[3]*Pharmacological Staff Room, School of Pharmacy, Nanjing University of Traditional Chinese Medicine, Nanjing, 210029, P. R. China*

[4]*Department of Gastroenterology, Nanjing Drum Tower Hospital, The Affiliated Hospital of Nanjing University Medical School, Nanjing, 210008, P. R. China*

*Correspondence: xiaolzhoou@sina.com (Xiao-Yun Mei) and 13601586102@163.com (Jun Cao)

DOI:10.31083/j.jin.2020.01.1226

Denervated-dependent skeletal muscle atrophy is a disease induced by skeletal muscle associated peripheral neuro-disconnection. Its specific molecular mechanisms remain unknown. The treating for denervated-dependent skeletal muscle atrophy is applied with an herbal complex Buyang Huanwu Tang used in traditional Chinese medicine and subjected to the established denervated-dependent skeletal muscle atrophy in rat models, and the therapeutic effects and associated mechanisms were evaluated in the pathogenesis of denervated-dependent skeletal muscle atrophy. Denervated-dependent skeletal muscle atrophy in rats was established and randomly divided into eight groups, including Normal control, Model, Positive control, Model + Buyang Huanwu Tang, Model + astragalus extracts, Model + Buyang Huanwu Tang-astragalus, Buyang Huanwu Tang + LY294002, and astragalus extract + LY294002 group. Hematoxylin-eosin staining and quantitative RT-PCR (qRT-PCR) assay were used to examine the inflammatory response of muscle tissues. Quantitative RT-PCR and Western blotting assay were utilized to analyze mRNA and protein expression. Immunohistochemistry assay was used to detect molecule expression in anterior cervical muscle tissues. Motor endplate activity was examined using the whole-mount acetylcholinesterase staining method. The wet mass ratio of anterior cervical muscle was measured. The results indicated that Buyang Huanwu Tang treatment significantly alleviated inflammatory response, enhanced acetylcholinesterase activity, and motor endplate functions, and promoted wet mass of anterior cervical muscle compared to denervated-dependent skeletal muscle atrophy rat models ($P < 0.05$). Buyang Huanwu Tang regulated molecules of PI3K/PKB/GSK3β/FOXO1 signaling pathway. Buyang Huanwu Tang significantly reduced muscle atrophy F-box protein, MuFR-1, Bax and caspase 9 expression, significantly enhanced Bcl-2 expression, and remarkably increased element-binding protein and vascular endothelial growth factor levels, compared to Model group ($P < 0.05$). Buyang Huanwu Tang suppressed caspase 9 and caspase 3 activity and associated apoptosis. Moreover, PI3K specific blocker, LY294002, significantly inhibited the effects of Buyang Huanwu Tang on the above molecule expression ($P < 0.05$). In conclusion, Buyang Huanwu Tang improved motor endplate functions of denervated-dependent skeletal muscle atrophy rat model through suppressing mitochondria-mediated apoptosis and activating PI3K/PKB/FOXO1 signaling pathway.

Keywords

Molecular mechanisms; denervated-dependent skeletal muscle atrophy; Buyang Huanwu Tang; PI3K; mitochondria-mediated apoptosis

1. Introduction

Denervated-dependent skeletal muscle atrophy (DSMA) is considered as a peripheral neurodisconnection induced disease of skeletal muscle (Tajrishi et al., 2014; Xiang et al., 2019). Clinically, the pharmacological or therapeutic medicine or drug treatment always induce the skeletal muscle atrophy (SMA), which causes destroy for voluntary-contractile effects on skeletal muscles or induces traumatic peripheral nerve injury (Nagpal et al., 2012; Zanella et al., 2018). The nerve injury usually complicates with a few symptoms, such as diabetic neuropathy, degenerative

Journal of Integrative Neuroscience

disc disease, SMA, trauma, alcoholic neuropathy, viral infection, and the cancers (Hsieh et al., 2011; Tamura et al., 2015). Therefore, when the symptoms of muscle denervation combining with several SMA-associated factors, DSMA is induced and causes the irreversible dysfunction of muscles, which can't be rescued with any treatment clinically (Huang et al., 2016; Li et al., 2016). Although there have been applied several therapeutic methods for treating DSMA nowadays (Huang et al., 2016; Romeo-Guitart et al., 2017), the therapeutic effects are also unsatisfactory.

Buyang Huangwu Tang (BYHWT) is a classical drug-formula in Traditional Chinese Medicine, which is derived from the Chinese-medicine theory known as "supplementing qi," creating back to 200 common Era (C.E.) (Zhang et al., 2010). BYHWT could promote blood-circulation, clear collaterals, remove blood stasis, treat vascular dementia, and cerebral ischemia-reperfusion (Liu et al., 2003). Furthermore, BYHWT could also effectively suppress activation of caspase, inhibit apoptosis, and modulate mitochondrial functions (Tang et al., 2006; Zhou et al., 2018). However, there are even no studies reporting the side-effects of BYHWT till now. Therefore, we hypothesize that the BYHWT might potentiate anti-neurotoxicity effects and promote the treatment of nerve injury in DSMA when administered.

2. Materials and methods

2.1 Rats and reagents

The male Sprague-Dawley (SD) rats, weighing from 180 to 220 g, aging from 8 to 10 weeks, were obtained from Huafukang BioSci. (Beijing, PRC). Male rats just because the male rats could illustrate more robust vitality and are easy to be operated on, as well as the muscles, could be easily isolated from male rats due to large in size and weight. The rats freely accessed to food and water at optimal humidity and room temperature. All tests or experiments were conducted based on the Guidelines of Institutional Animal Care. Meanwhile, this study was also approved by the Ethics Committee of Traditional Chinese Medicine in Nanjing University.

Buyang Huangwu Tang was mainly composed of Rhizoma Chuanxiong (12 g), Peach seeds (12 g), Astragalus (480 g), Pheretima (12 g), Tangkuei tail (24 g), Red flower (12 g), Paeoniae (20 g), all of which were purchased from Tongrentang Co. Ltd. (Beijing, PRC). These ingredients were treated, mixed, and purified according to our previously published study (Zhou et al., 2018). Chemical reagents involving in BYHWT production, including $MgCl_2$, K_3PO_4, and K_2HPO_4, were obtained from Chengdu Kelong Co. Ltd.

2.2 DSMA model establishment

A total of 35 SD rats were collected to establish DSMA models, and the other 5 rats were defined as the normal control group. Briefly, SD rats were anesthetized by injecting intraperitoneally with 7% chloral hydrate (at a final concentration of 0.5 ml/100 g body weight). In short detailed processes for establishing the DSMA model were conducted according to our previously published report (Zhou et al., 2018). The model establishment processes and sample isolating processes mainly included the following items: anesthesia, rat peroneal nerve injury, seaming, intragastric administration, intramuscular injection, cut-off skin fascia, tibialis anterior muscle isolation, shear-off tibialis anterior muscle and washing of tibialis anterior muscle.

2.3 Experimental grouping and administration

Established DSMA rats were classified into seven groups (n = 5 for each group): Model group, positive control group (n = 5) (intragastric administration with mecobalamin coated tablet at final concentration of 625 μg/kg body weight), Model + BYHWT group (doubling diluted BYHWT stock solution, intragastric administration, 2 ml every day), Model + astragalus extracts (4-folds diluted astragalus extracts stock solution, intragastric administration, 2 ml every day), Model + BYHWT-astragalus (same with Model + BYHWT group, without component of astragalus, intragastric administration, 2 ml every day), BYHWT + LY294002 group (same with Model + BYHWT group, additionally intramuscular injecting with PI3K specific blocker, LY294002 (Beyotime Biotech. Shanghai, China), at final concentration of 30 μmol/l), and Astragalus extract + LY294002 group (same with Model + astragalus extracts group, additionally intramuscular injecting with LY294002, at final concentration of 30 μmol/l).

2.4 Wet mass ratio of anterior cervical muscle

The anterior cervical muscle was incised and then completely removed from rats. An electronic balance was applied to the wet weight mass of anterior cervical muscle. Subsequently, the wet mass ratio of anterior cervical muscle was calculated as Wet mass ratio = wet mass of anterior cervical muscle/contralateral wet mass of anterior cervical muscle. Post weighting the anterior cervical muscle mass, the isolated muscles were stored at -80 °C for the other experiments.

2.5 Hematoxylin-eosin (HE) staining

Anterior cervical muscle tissues were isolated and fixed using 4% formaldehyde in phosphate-buffered saline (PBS, Sigma-Aldrich). Then, the histology was evaluated and visualized with the HE staining method, as the previous report documented (Tian et al., 2017). HE stained anterior cervical muscle tissues that were demonstrated and captured with an AX70 digital microscope (Olympus, Tokyo, Japan). Magnification of digital graphs, 100 ×.

2.6 Quantitative RT-PCR (qRT-PCR)

The RNAs in isolated anterior cervical muscles were extracted with Trizol reagents based on the instruction of the manufacturer. The complementary DNA (cDNA) was synthesized with the RNAs as a template by employing the ImProm-II Reverse-Transcription system (Cat. No. A3800, Promega, Madison, MI, USA) based on the manufacturer's instruction. The systematic volume for this qRT-PCR assay was 10 μl, which was composed of cDNA template (1 μl), 2 × SYBR Green Mixture (4.5 μl), forward and reverse primers (1 μl, respectively) and ddH2O (2.5 μl). qPCR was conducted according to the followings processes: 94 °C (4 min), 94 °C (20 s), 60 °C (30 s), 72 °C (30 s), for a total of 35 cycles, and was terminated at 72 °C for 10 min, for 35 cycles. qRT-PCR was conducted using Eppendorf Master PCR cycler (Mode: X50 h, Eppendorf, Wesseling-Berzdorf, Germany) for 40 cycles. The qRT-PCR primers were listed in Table 1, and the glyceraldehyde phosphate dehydrogenase (GAPDH) was employed as an internal control. Gene expressions were quantified relative to GAPDH expression with an optimized comparative cycle threshold (Ct) ($2^{-\triangle Ct}$) approach (Livak and Schmittgen, 2001), where "$\triangle Ct$" represents the difference between the objective gene Ct value and the internal reference gene Ct value.

Table 1. Primers for the quantitative RT-PCR.

Gene		Primers
Bcl-2	forward	GTGAACTGGGGGAGGATTGT
	reverse	GCATCCCAGCCTCCGTTA
Bax	forward	CCGAGTGAGCAGGAAGACG
	reverse	GTTATTGGCTGCCTGTCCC
caspase 9	forward	GCCAGATGCTGTCCCATACC
	reverse	CCAGGAACCGCTCTTCTTGT
CREB	forward	GCCAACCCCGATTTACCA
	reverse	GGGCACTAGAATCTGCTGTCC
VEGF	forward	CAAAGCCAGCACATAGGAGAGA
	reverse	CTATCTTTCTTTGGTCTGCATTCAC
CD11b	forward	CAGCCTTTGACCTTATGTCATGG
	reverse	CCTGTGCTGTAGTCGCACT
CD16	forward	ATGTGTCTTCAGAGACTGTGAAC
	reverse	TTTATGGTCCTTCCAGTCTCTTG
GAPDH	forward	CCCATCTATGAGGGTTACGC
	reverse	TTTAATGTCACGCACGATTTC

2.7 Western blotting assay

Radioimmunoprecipitation assay (RIPA) was used to lysed anterior cervical muscles, the products of which were centrifuged at 12000 $\times$ g for 20 min. The obtained supernatant was separated with 10% sodium dodecyl sulphate-polyAcrylamide gel electrophoresis (SDS-PAGE) and transferred onto polyvinylidene fluoride (PVDF) membrane (purchasing from DuPont, Wilmington, DE, USA) by employing the electronic-transferred instrument (Bio-Rad., Hercules, CA, USA). Electronic-transferred PVDF membranes were blocked with 5% skimmed for 120 min at 37 °C. PVDF were treated using rabbit anti-rat mammalian target of rapamycin (mTOR) polyclonal antibody (Cat. No. ab2732, 1: 2000), rabbit anti-rat phosphorylated PI3K (p-PI3K) polyclonal antibody (Cat. No. ab182651, 1: 2000), mouse anti-rat muscle ring finger 1 (MURF1) polyclonal antibody (Cat. No. ab172479, 1: 3000), rabbit anti-rat phosphorylated forkhead box protein O1 (FOXO1) monoclonal antibody (Cat. No. ab52857, 1: 3000), rabbit anti-rat phosphorylated protein kinase B (p-PKB) polyclonal antibody (Cat. No. ab38513, 1: 2000), rabbit anti-rat GSK3β polyclonal antibody (Cat. No. ab131356, 1: 2000), muscle atrophy F-box protein (MAFBX) polyclonal antibody (Cat. No. ab74023, 1: 2000), rabbit anti-rat Bcl-2 polyclonal antibody (Cat. No. ab196495, 1: 2000), rabbit anti-rat Bax monoclonal antibody (Cat. No. ab32503, 1: 3000), rabbit anti-rat caspase 9 monoclonal antibody (Cat. No. ab184786, 1: 3000), rabbit anti-rat cAMP-response element binding protein (CREB) monoclonal antibody (Cat. No. ab32515, 1: 30000), rabbit anti-rat vascular endothelial growth factor (VEGF) polyclonal antibody (Cat. No. ab231260, 1: 2000) and rabbit anti-rat GAPDH polyclonal antibody (Cat. No. ab9485, 1: 2000) at 4 °C overnight. All of the above listed primary antibodies were purchased from Abcam Biotech. (Cambridge, Massachusetts, USA). The primary antibodies labeled PVDF membranes were washed with phosphate-buffered saline Tween-20 (PBST) for 5 min per time and 3 times. The washed PVDF were treated using HRP-conjugated goat anti-mouse IgG (1: 1000, Sigma-Aldrich, St. Louis, Missouri, USA) and HRP-conjugated goat anti-rabbit IgG (1: 1000, Sigma-Aldrich, USA) at 37 °C for 60 min, and then washed using PBST for 3 times (5 min per time). Finally, ECL reagent, which was purchased from Thermo Scientific Pierce (Rockford, IL, USA), was utilized to incubate the PVDF membrane in the dark for 2 min. Relative grey density (by grey scanning) of western blot bands were evaluated and analyzed with Labworks TM Analysis Software (Labworks, Upland, CA, USA).

2.8 Immunohistochemistry analysis

Anterior cervical muscle tissue was treated and fixed using 4% paraformaldehyde (Sigma-Aldrich) for 20 min. Then, anterior cervical muscle tissue was sliced into the thickness and inactivated using 3% hydrogen peroxide (Beyotime Biotech. Shanghai, PRC) at room temperature for 10 min. The sections were incubated with antibodies of mTOR, p-PI3K, p-FOXO1, p-PKB, GSK3β, MAFBX, and MuRF-1 at 4 °C overnight. The anterior cervical muscle sections were incubated with Biotin-labeled goat anti-mouse or the goat anti-rabbit IgG (Sigma-Aldrich) according to instructions of manufacturers. Finally, the images of stained anterior cervical muscle slices were observed using the AX70 inverted microscope (Olympus, Japan) and analyzed using an Image-Pro Plus software 6.0, which was purchased from Media Cybernetics Inc. (Bethesda, MD, USA).

2.9 Motor endplates examination

Isolated anterior cervical muscles were stained using wholemount acetylcholinesterase (AChE) staining to exhibit motor endplates activity. Briefly, anterior cervical muscles were dissected freely using a dissecting microscope. Post gross anatomical characteristics were observed, anterior cervical muscles were stained using AChE staining to delineate localization and distribution of motor endplates. Briefly, wholemount AChE staining processes were conducted based on the previous study described (Zhang et al., 2011).

2.10 Caspase 3 and caspase 9 activity assay

Here, the caspase 3 and caspase 9 activity was measured using caspase 3 activity assay kit (Cat. No. C1115, Beyotime Biotech. Shanghai, PRC) and caspase 9 activity assay kit (Cat. No. C1158, Beyotime Biotech. Shanghai, PRC), according to protocols of manufacturers. In brief, the anterior cervical muscles were lysed using lysis buffer. The above lysates were centrifuged at a speed of 10000 r/min, and the supernatants were transferred to tubes for examining caspase activity. The buffer solution, above samples and the Ac-DEVD-pNA, were added to the 96-well plates and incubated for 2 h at room temperature. Finally, the A405 wavelength recordings were immediately when illustrating noticeable changes of color, which could reflect the caspase 3 or caspase 9 activity for the above samples.

2.11 Statistical analysis

The data analysis was conducted with the professional SPSS software (version: 20.0, SPSS Inc., Chicago, Ull, USA) and presented as mean $\pm$ SD. All of the data were confirmed at least by conducting 3 independent tests. The student's t-test was utilized to analyze the significant difference between the two groups. The Tukey's posthoc test validated ANOVA was employed to analyze substantial differences among the multiple groups. The value of $P < 0.05$ was assigned as a statistical significance.

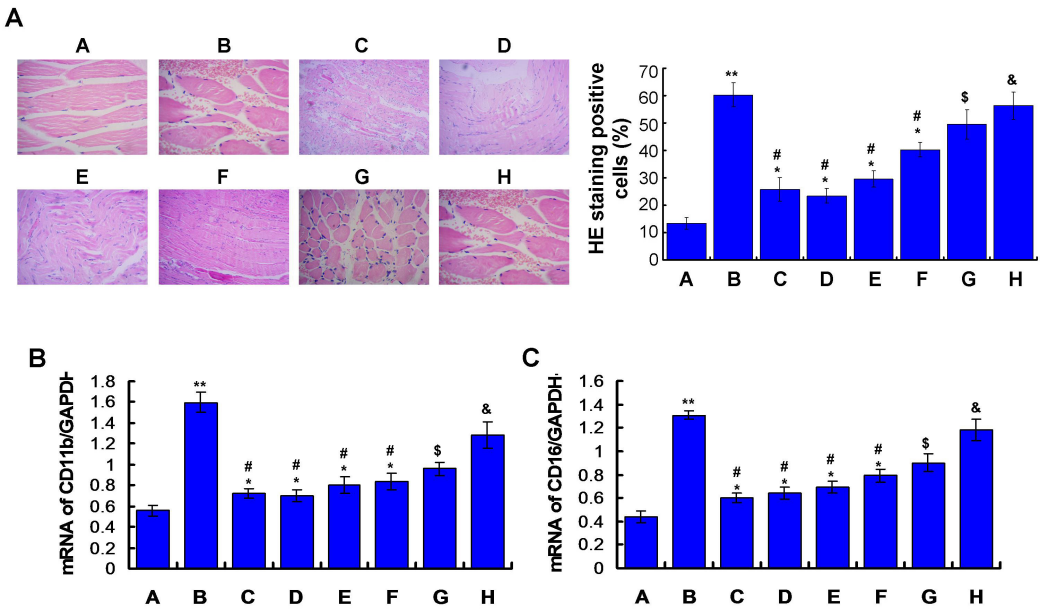

Figure 1. Evaluation of the inflammatory response in anterior cervical muscle tissues of DSMA rat models (n = 5 for each group). A. HE staining and statistical analysis for observing inflammation. B. Determination and statistical analysis for inflammatory response marker CD11b using RT-PCR assay. C. Determination and statistical analysis for inflammatory response marker CD16 using RT-PCR assay. $^{*}P < 0.05$ vs. Normal, $^{\#}P < 0.05$ vs. Model, $^{\$}P < 0.05$ vs. BYHWT, $^{\&}P < 0.05$ vs. Astragalus. For every group, A: Normal control group, B: Model group, C: positive control, D: Model + BYHWT group, E: Model + astragalus extracts, F: Model + BYHWT astragalus group, G: BYHWT + LY294002 group, H: Astragalus extracts + LY294002 group.

3. Results

3.1 BYHWT administrated alleviated inflammatory response in DSMA rat models

The HE staining findings showed that the BYHWT treatment, astragalus treatment, and BYHWT-astragalus treatment reduced the inflammatory cell amounts significantly compared to that in the Model group (Fig. 1A, $P < 0.05$). Moreover, PI3K specific blocker, LY294002, significantly blocked the effects of BYHWT (or astragalus) compared to the BYHWT treatment group (or astragalus treatment group) (Fig. 1A, $P < 0.05$).

Moreover, the inflammatory response specific markers, CD11b and CD16 molecules were also examined using RT-PCR assay. The results showed that both CD11b and CD16 molecules were highly expressed in the Model group (Fig. 1B). However, the expressions were decreased undergoing the treatment of BYHWT, Astragalus, and BYHWT-combining the astragalus group (Fig. 1B). Statistical analysis indicated that BYHWT treatment, Astragalus treatment, and BYHWT combining astragalus treatment significantly reduced expressions of CD11b and CD16 compared to that in Model group (Fig. 1B, $P < 0.05$). Meanwhile, among the above three treatments, BYHWT exhibited the most significant inhibitive effects on the expression of CD11b and CD16 (Fig. 1B). Meanwhile, LY294002 also significantly blocked the impact of BYHWT (or astragalus) on CD11b and CD16 expression compared to that of the BYHWT treatment group (or astragalus treatment group) (Fig. 1B, $P < 0.05$).

3.2 BYHWT enhanced acetylcholinesterase activity and motor endplate functions

To evaluate motor endplate functions, AChE activity was examined (Fig. 2A). The results demonstrated that the activity of AChE was remarkably decreased in the Model group comparing to that in the Normal control group (Fig. 2B, $P < 0.05$). However, BYHWT treatment, Astragalus treatment, BYHWT-astragalus treatment remarkably enhanced AChE activity comparing to that in the Model group (Fig. 2B, $P < 0.05$), among which BYHWT illustrated the higher effects. Moreover, LY294002 significantly inhibited the BYHWT triggered enhancement of AChE activity in both BYHWT + LY294002 and Astragalus extracts + LY294002 group (Fig. 2B, $P < 0.05$).

3.3 BYHWT increased wet mass of muscles

To further clarify the effects of BYHWT on muscle atrophy, the wet mass ratio of muscle was measured. The results showed the wet mass ratio was remarkably reduced in the Model group compared to that in the normal control group (Fig. 3, $P < 0.05$). The BYHWT treatment, Astragalus treatment, BYHWT-astragalus treatment significantly increased wet mass ratio compared to that in the Model group (Fig. 3, $P < 0.05$), among which BYHWT demonstrated the higher effects. Furthermore, LY294002 significantly suppressed BYHWT triggered an increase of wet mass ratio in both BYHWT + LY294002 and Astragalus extracts + LY294002 group (Fig. 3, $P < 0.05$).

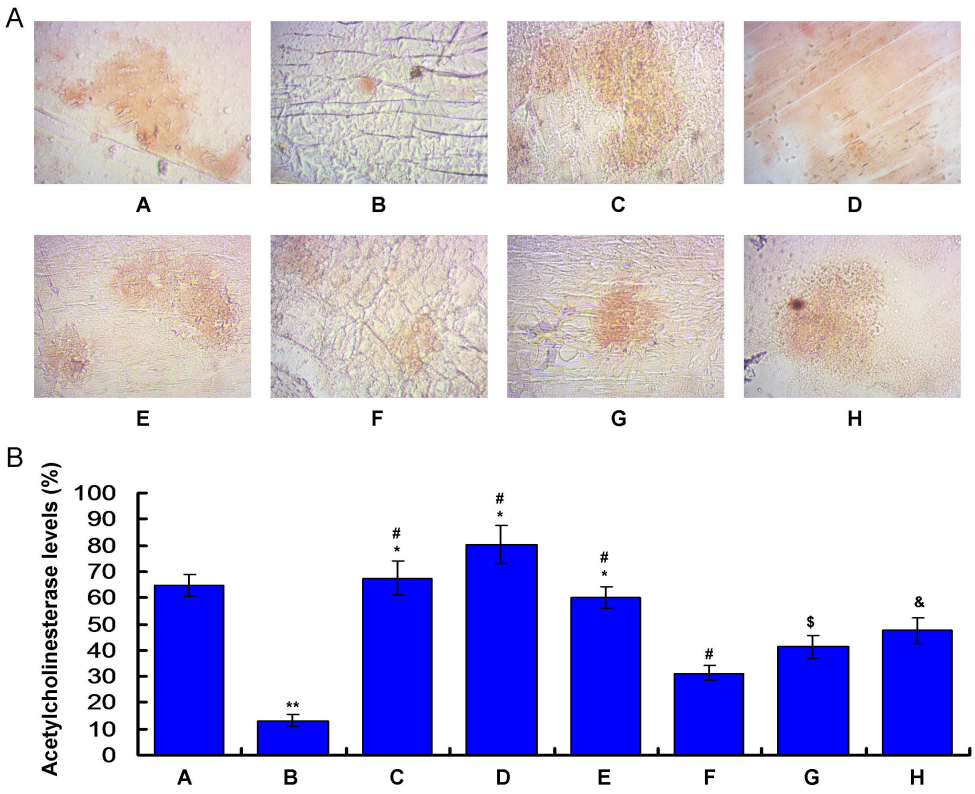

Figure 2. Investigation for effects of BYHWT on motor endplate functions by examining acetylcholinesterase activity (n = 5 for each group). A. Images for the acetylcholinesterase staining. B. Data analysis of acetylcholinesterase staining in each group. $^{*}P < 0.05$ vs. Normal, $^{\#}P < 0.05$ vs. Model, $^{\$}P < 0.05$ vs. BYHWT, $^{\&}P < 0.05$ vs. Astragalus. A: Normal control group, B: Model group, C: positive control, D: Model + BYHWT group, E: Model + astragalus extracts, F: Model + BYHWT astragalus group, G: BYHWT + LY294002 group, H: Astragalus extracts + LY294002 group.

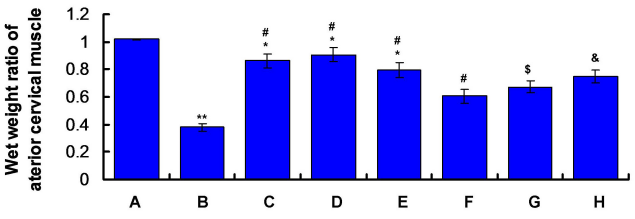

Figure 3. The wet mass ratio of aterior cervical muscles in all groups (n = 5 for each group). $^{*}P < 0.05$ vs. Normal, $^{\#}P < 0.05$ vs. Model, $^{\$}P < 0.05$ vs. BYHWT, $^{\&}P < 0.05$ vs. Astragalus. A: Normal control group, B: Model group, C: positive control, D: Model + BYHWT group, E: Model + astragalus extracts, F: Model + BYHWT astragalus group, G: BYHWT + LY294002 group, H: Astragalus extracts + LY294002 group.

3.4 BYHWT regulated molecules of PI3K/PKB/GSK3β/FOXO1 signaling pathway

To clarify the mechanism for BYHWT triggered inflammation inhibition and AChE activity enhancement, the molecule levels of PI3K/PKB/FOXO1 signaling pathway were evaluated (Fig. 4A). The findings illustrated that mTOR levels were significantly increased in Model, BYHWT, Astragalus, BYHWT-astragalus administrated group comparing to that in the Normal control group, however, significantly decreased compared to both BYHWT + LY294002 and Astragalus extracts + LY294002 group (Fig. 4B, $P < 0.05$). Meanwhile, BYHWT treatment significantly increased ratio of p-PI3K/PI3K, ratio of p-PKB/PKB and GSK3β expression and decreased considerably ratio of p-FOXO1/FOXO1 compared to Model group (Fig. 4C, D, E, F, $P < 0.05$), however, the effects of which were significantly suppressed by PI3K specific blocker, LY294002 ($P < 0.05$). Although the Astragalus treatment and BYHWT-astragalus treatment groups also regulated the ratio of p-PI3K/PI3K, p-FOXO1/FOXO1, p-PKB/PKB, and GSK3β expression, the effects of which were significantly weaken compared to BYHWT treatment (Fig. 4C, D, E, $P < 0.05$).

3.5 BYHWt treatment reduced the expression of MAFBX and MuFR-1 expression

The skeletal muscle atrophy specific molecules, MAFBX, and MuRF-1 (Rom and Reznick, 2016), were examined using western blots. The results showed that both MAFBX and MuRF-1 levels were increased remarkably in Model group comparing to that in the Normal control (Fig. 4G,H, $P < 0.05$). MAFBX (Fig. 4G) and MuRF-1 (Fig. 4H) levels were significantly decreased in BYHWT, Astragalus, BYHWT-astragalus treatment group, compared to that in the Model ($P < 0.05$). Also, BYHWT illustrated the high-

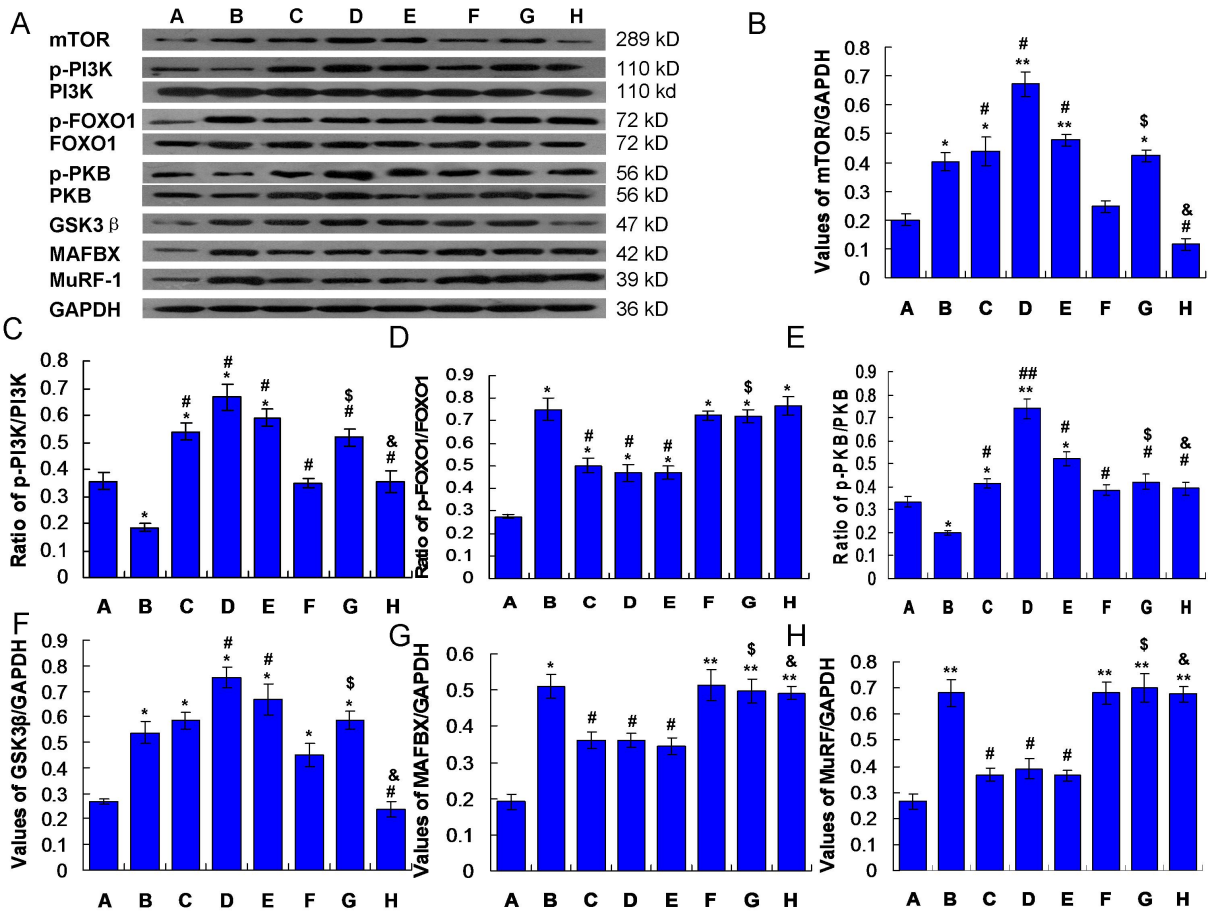

Figure 4. Examination for protein expression in anterior cervical muscle samples of DSMA rat models using western blot assay (n = 5 for each group). A. Western blot bands and images for proteins. Statistical analysis for mTOR expression (B), p-PI3K/PI3K ratio (C), p-FOXO1/FOXO1 ratio, (D) p-PKT/PKB ratio (E), GSK3β expression (F), MAFBX expression (G) and MuRF-1 expression (H) were also conducted. $^{*}P < 0.05$ vs. Normal, $^{\#}P < 0.05$ vs. Model, $^{\$}P < 0.05$ vs. BYHWT, $^{\&}P < 0.05$ vs. Astragalus. For every group, A: Normal control group, B: Model group, C: positive control, D: Model + BYHWT group, E: Model + astragalus extracts, F: Model + BYHWT astragalus group, G: BYHWT + LY294002 group, H: Astragalus extracts + LY294002 group.

est levels of MAFBX and MuRF-1 among all of the above three groups (Fig. 4G,H). Moreover, PI3K specific blocker, LY294002, significantly suppressed the BYHWT triggered reduced levels of MAFBX and MuRF-1 in both BYHWT + LY294002 and Astragalus extracts + LY294002 group (Fig. 4G,H, $P < 0.05$).

Furthermore, the immunohistochemistry assay results also showed that BYHWT significantly increased levels of mTOR, p-PI3K, p-PKB, GSK3β, and decreased levels of p-FOXO1, MAFBX and MuRF-1 compared to that in Model group (Fig. 5, $P < 0.05$). Moreover, PI3K specific blocker, LY294002, significantly inhibited the effects of BYHWT on the expression of the above molecules (Fig. 5, $P < 0.05$).

3.6 BYHWT up-regulated Bcl-2 and down-regulated Bax expression

To clarify the cause for the injury of skeletal muscle atrophy, the critical biomarkers for mitochondrial associated signaling pathway, Bcl-2, and Bax (Zhao et al., 2017), were evaluated in the present research (Fig. 6A). Our findings demonstrated that Bcl-2 levels (Fig. 6B) in the Model group were decreased remarkably, and Bax levels (Fig. 6C) were remarkably increased compared to that in the Normal control ($P < 0.05$). Meanwhile, both higher and lower dosage of LY294002 treatment significantly inhibited the effects of BYHWT on both Bcl-2 (Fig. 6B) and Bax (Fig. 6C) ($P < 0.05$).

3.7 BYHWT inhibited caspase 9 expression

Because the BYHWT triggered the modulation of Bcl-2 and Bax participated, the apoptosis-associated pathway was investigated. The results showed that the caspase 9 expression was up-regulated remarkably in Model group comparing to that in the Normal control group (Fig. 6D). BYHWT treatment significantly decreased caspase 9 expressions compared to that in the Model group (Fig. 6D, $P < 0.05$). However, the effects of which were significantly inhibited by the treatment of both higher and lower dosage of LY294002 (Fig. 6D).

3.8 BYHWt enhanced expression of CREB

As all known, the skeletal muscle growth and apoptosis are associated with the CREB expression according to the previous study (Zuo et al., 2015). The results indicated that CREB levels were down-regulated remarkably in the Model group compared to that in the normal control group (Fig. 6E, $P < 0.05$). BYHWT

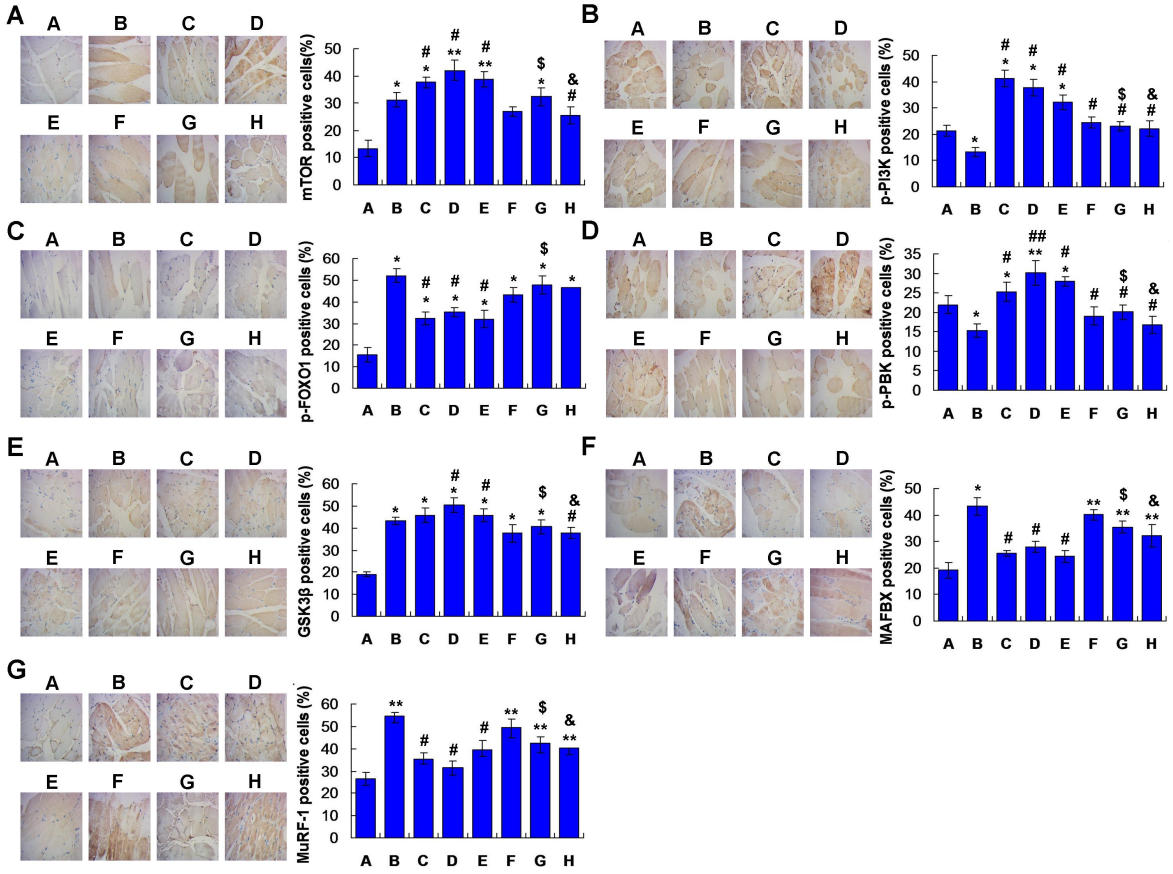

Figure 5. Evaluation for mRNA expression in anterior cervical muscle samples of DSMA rat models using qRT-PCR assay (n = 5 for each group). Here, we conducted the statistical analysis for mTOR expression (A) p-PI3K expression (B), p-FOXO1 expression (C), p-PKB expression (D), GSK3β expression (E), MAFBX expression (F) and MuRF-1 expression (G). $^{*}P < 0.05$ vs. Normal, $^{\#}P < 0.05$ vs. Model, $^{\$}P < 0.05$ vs. BYHWT, $^{\&}P < 0.05$ vs. Astragalus.For every group, A: Normal control group, B: Model group, C: positive control, D: Model + BYHWT group, E: Model + astragalus extracts, F: Model + BYHWT astragalus group, G: BYHWT + LY294002 group, H: Astragalus extracts + LY294002 group.

treatment significantly enhanced the levels of CREB compared to that in the Model group (Fig. 6E, $P < 0.05$). Meanwhile, PI3K specific blocker, LY294002, significantly inhibited the effects of BYHWT on CREB levels (Fig. 6E).

3.9 BYHWt increased expression of VEGF

The skeletal muscle growth is correlated with the VEGF expression due to the previously published report (Du et al., 2018). Our results illustrated that BYHWT treatment remarkably enhanced VEGF levels that reduced in the Model group (Fig. 6F, $P < 0.05$). Meanwhile, the PI3K specific blocker, LY294002, significantly suppressed the effects of BYHWT on the VEGF expression (Fig. 6F).

Moreover, the RT-PCR results also showed that BYHWT treatment significantly enhanced Bcl-2, CREB, VEGF levels, and reduced Bax considerably and caspase 9 levels, compared to that in Model group (Fig. 7, $P < 0.05$). Also, PI3K specific blocker, LY294002, significantly inhibited the effects of BYHWT on the expression of the above molecules (Fig. 7).

3.10 BYHWT suppressed Caspase 9 and Caspase 3 activity

The results showed that the caspase 9 activity was significantly increased compared to that in the normal control group (Fig. 8A). BYHWT treatment significantly decreased caspase 9 activity compared to that in the Model group (Fig. 8A, $P < 0.05$). However, the effects of which were significantly inhibited by treatment of both higher and lower dosage of LY294002 (Fig. 8A). Moreover, BYHWT treatment also considerably reduced the caspase 3 activity compared to that in the Model group (Fig. 8B, $P < 0.05$). Meanwhile, LY294002 suppressed the effects of BYHWT on the caspase 3 activity (Fig. 8B).

4. Discussion

The most significant conclusion from our research is that BYHWT treatment plays an essential role in treating denervation caused muscle atrophy of DSMA rat models. BYHWT exhibited substantial neuroprotective roles, nerve-function improving functions, and anti-ischemic stroke effects (Wei et al., 2013). Our previous study (Zhao et al., 2017; Zhou et al., 2018) reported that BYHWT participates in improvements of denervation-dependent muscle atrophy in DSMA models. Moreover, in another study, we also indicated that BYHWT could improve the motor endplate function of DSMA rats through activating cellular response to the interferon-gamma, integral component of the plasma membrane, and voltage-gated potassium channel activity genes and

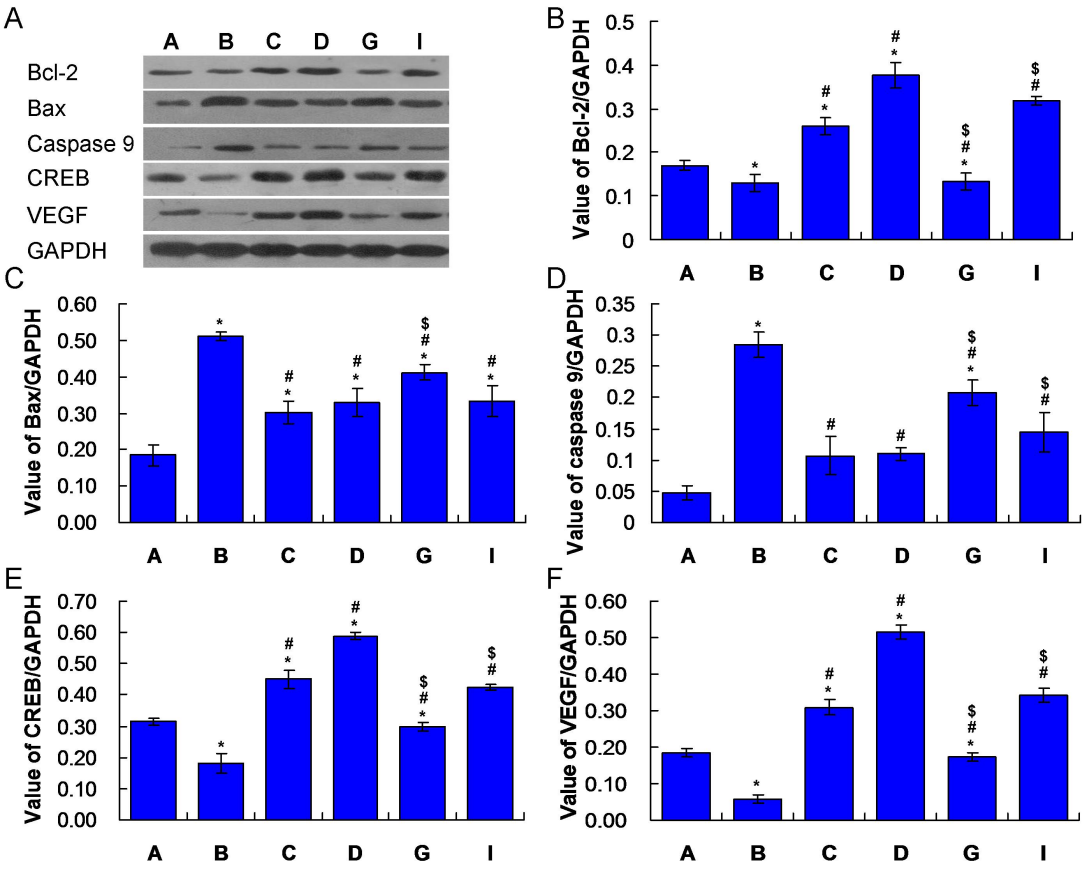

Figure 6. Examination for Bcl-2, Bax, caspase 9, CREB, and VEGF expression in anterior cervical muscle samples of DSMA rat models using western blotting analysis (n = 5 for each group). A. Western blot bands and images for proteins. Data analysis of Bcl-2 expression (B), Bax expression (C), caspase-9 expression (D), CREB expression (E), VEGF expression (F) were also conducted. $^{*}P < 0.05$ vs. Normal, $^{\#}P < 0.05$ vs. Model, $^{\$}P < 0.05$ vs. BYHWT. For every group, A: Normal control group, B: Model group, C: positive control, D: Model + BYHWT group, G: BYHWT + LY294002 (30 μmol/l) group, I: BYHWT + LY294002 (15 μmol/l) group.

associated signaling pathways. However, the specific signaling pathway and related molecules were not clarified (Zhou et al., 2019). Therefore, in this paper, we showed BYHWT potentiates the anti-neurotoxicity effects and promotes nerve injury treatment in DSMA rats through mitochondria-mediated apoptosis and PI3K/PKB/FOXO1 signaling pathway.

To evaluate the injury of skeletal muscle, the inflammatory response was also assessed with HE staining and RT-PCR assay. The HE staining results showed that HE-positive stained cells in the Model group were more significantly compared to that in the Normal control group. However, the BYHWT, Astragalus, and BYHWT-astragalus significantly decreased the HE staining cells, among which BYHWT exhibited the most apparent effects on the inflammatory response. The RT-PCR assay also illustrated that BYHWT, Astragalus, and BYHWT-astragalus significantly enhanced CD11b and CD16 expression, among which BYHWT demonstrated the most significant effects on the inflammatory response. These results suggest that BYHWT effectively inhibited the nerve injury associated with inflammation in DSMA rat models.

The morphology and activity of motor endplates reflect the status of skeletal muscle, and which could be evaluated by examining AChE (Nakata et al., 2013). The results showed that the AChE activity of the Model group was reduced remarkably comparing to that in the Normal control group, and which was significantly enhanced undergoing the BYHWT treatment. These results suggest that BYHWT could improve the function and activity of motor endplates. Moreover, compared to the Astragalus and BYHWT-astragalus group, BYHWT demonstrated the higher effects on the wet mass ratio of anterior cervical muscle. While LY294002 remarkably suppressed, BYHWT triggered an increase of wet mass ratio. These findings suggest that BYHWT could enhance the weight of muscles and might further promote the growth of muscles. Therefore, BYHWT may be a promising therapeutic target for the DSMA treatment in clinical.

To discuss the specific mechanisms or the signaling pathway that mediates the effects of BYHWT, PI3K/PKB/FOXO1 signaling pathway molecules (Law et al., 2013) were examined in isolated muscle tissues. The present results showed that BYHWT significantly increased levels of mTOR enhanced ratio of p-PI3K/PI3K, p-PKB/PKB, GSK3β, and the remarkably down-regulated ratio of p-FOXO1/FOXO1 compared to that in the Model group. Our result hints that BYHWT plays anti-inflammation and improving the activity of motor endplates by triggering the

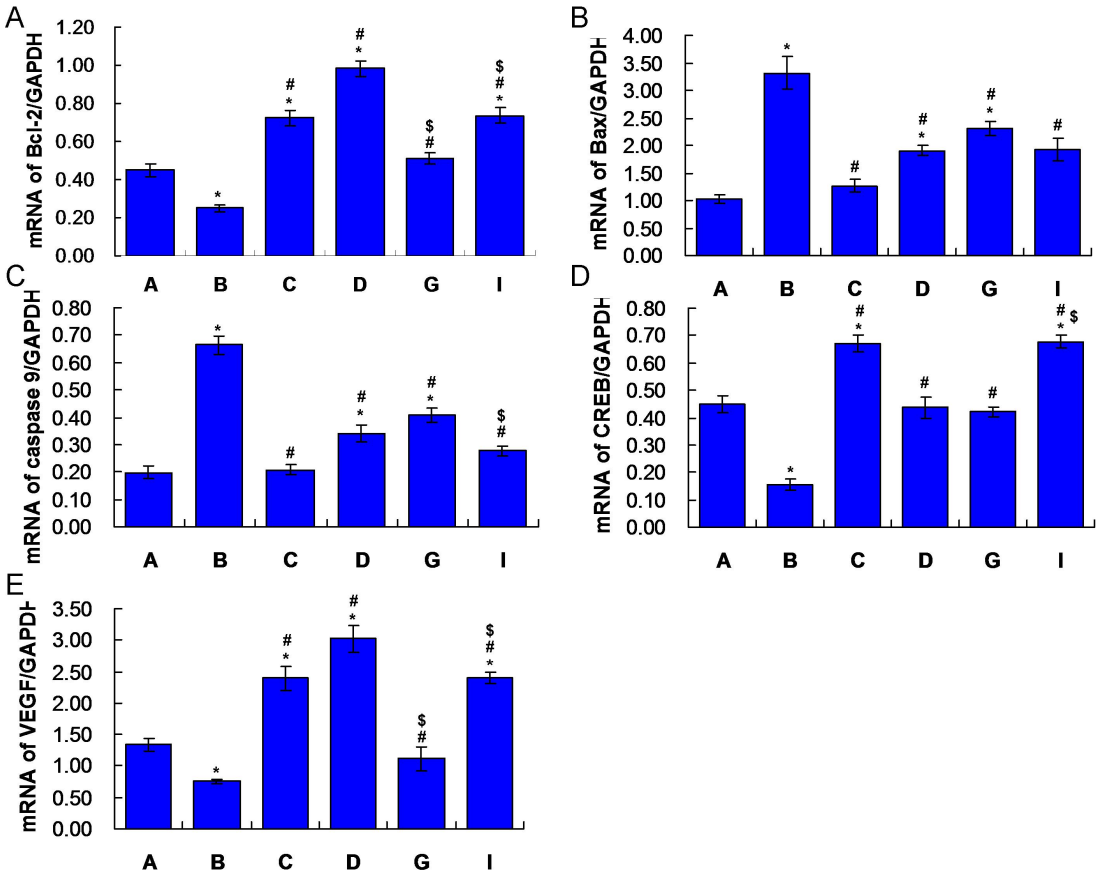

Figure 7. Evaluation for Bcl-2, Bax, caspase 9, CREB, and VEGF mRNA expression in anterior cervical muscle samples of DSMA rat models using qRT-PCR assay (n = 5 for each group). We also made the statistical analysis for Bcl-2 mRNA expression (A) Bax mRNA expression (B), caspase 9 mRNA expression (C), CREB mRNA expression (D), and VEGF mRNA expression (E). $^{*}P < 0.05$ vs. Normal, $^{\#}P < 0.05$ vs. Model, $^{\$}P < 0.05$ vs. BYHWT. For every group, A: Normal control group, B: Model group, C: positive control, D: Model + BYHWT group, G: BYHWT + LY294002 (30 μmol/l) group, I: BYHWT + LY294002 (15 μmol/l) group.

PI3K/PKB/FOXO1 associated signaling pathway. Moreover, we also discovered that levels of skeletal muscle atrophy specific molecules, MAFBX and MuRF-1, (Rom and Reznick, 2016) in were also decreased undergoing the treatment of BYHWT compared to the Model group. This result is consistent with the changes and findings of the inflammatory response and activity of motor endplates of the BYHWT results. Meanwhile, these results suggest that BYHWT reliably inhibits damage of muscle tissues and plays protective roles in DSMA rat models. Moreover, to clarify the pathway that mediated the effects of BYHWT, PI3K specific blocker, LY294002, was also employed. Undergoing the treatment of LY294002, effects of BYHWT on mTOR, p-PI3K/PI3K, p-PKB/PKB, GSK3β, p-FOXO1/FOXO1, MuRF-1, and MAFBX, were evaluated. The results showed that BYHWT might play anti-DSMA roles through inhibiting or blocking PI3K expression and further suppressing PI3K/PKB/FOXO1 associated signaling pathways.

Furthermore, to analyze the down-stream factors that caused muscle damage or injury in DSMA rat models, the mitochondria-mediated apoptosis signaling pathway was also investigated. As all known, both Bcl-2 and Bax are the classical and critical biomarker for the mitochondria-mediated apoptosis (Zhao et al., 2017), and which could activate the caspase family proteins and induce apoptosis (Chen et al., 2017). We found that BYHWT treatment significantly enhanced Bcl-2 expression and reduced Bax expression comparing to that in the Model group. Also, caspase-9 levels were decreased considerably, underwent BYHWT treatment compared to the model group. Moreover, due to caspase 3 and caspase 9 activity in tissues represents the activation of cleaved caspase 3 and caspase 9. Therefore, we examined caspase 3 and caspase 9 activity. The results indicated that BYHWT also significantly suppressed caspase 9 and caspase 3 activity. Thus, BYHWT could suppress the caspase 9 and caspase 3 mediated apoptosis. These results hint that damage of muscle in DSMA rat models was mediated by the mitochondria-associated apoptosis, which is firstly discovered compared to the published reports.

Similarly, we blocked the PI3K pathway by treating with LY294002 and found that PI3K molecules or associated signaling pathways also mediated the effects of BYHWT on Bcl-2 and Bax. As well, another apoptosis-associated biomarker for the muscle, CREB (Zuo et al., 2015), was also examined. Our results indicated that the down-regulated CREB expression in the Model group was significantly enhanced by BYHWT treatment, which suggests that BYHWT inhibits apoptosis also through CREB associated sig-

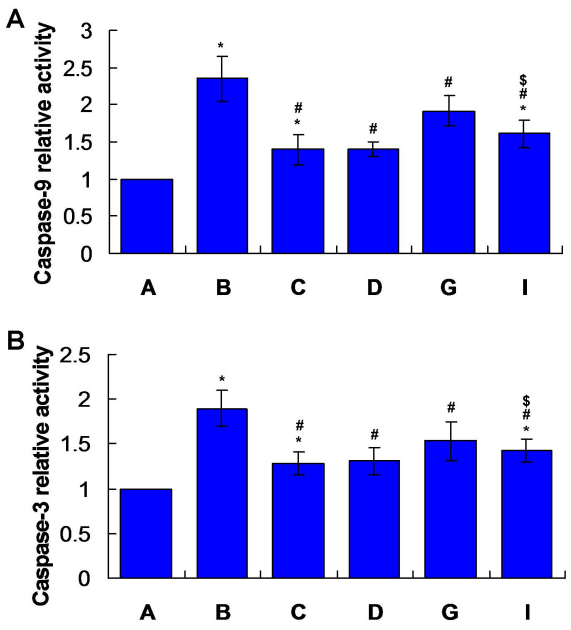

Figure 8. BYHWT inhibited caspase 3 activity and caspase 9 activity in anterior cervical muscle samples of DSMA rat models (n = 5 for each group). A. Statistical analysis for caspase 9 activity. B. Statistical analysis for caspase 3 activity. $^{*}P < 0.05$ vs. Normal, $^{\#}P < 0.05$ vs. Model, $^{\$}P < 0.05$ vs. BYHWT. For every group, A: Normal control group, B: Model group, C: positive control, D: Model + BYHWT group, G: BYHWT + LY294002 (30 μmol/l) group, I: BYHWT + LY294002 (15 μmol/l) group.

naling pathway. Interestingly, PI3K blocking substantially block CREB mediated apoptosis signaling pathway in DSMA rat models and the specific mechanism of which would be explored in the following study. Moreover, the potential molecules that activate the PI3K molecule have not been examined. In subsequent research, we aim to investigate the possible mechanism behind BYHWT, through examining molecules activating PI3K molecule.

Rrey et al. (2012) and Cheng et al. (2016) reported that VEGF plays an essential role in the repair of muscle tissues. Therefore, we investigated the effects of BYHWT on the expression of VEGF in DSMA rat models and found that BYHWT remarkably enhanced levels of VEGF compared to that in the DSMA model. The finding hints that BYHWT improves the conditions of skeletal muscle by triggering VEGF expression, which is consistent with the previously published study (Zhang et al., 2010).

5. Conclusions

Buyang Huanwu Tang inhibited the DSMA by inhibiting the mitochondria-mediated apoptosis and activating the PI3K/PKB/FOXO1 signaling pathway. The present findings provided the empirical basis and research direction for exploring the specific mechanisms through which Buyang Huanwu Tang improves the motor activity and inhibits denervated-dependent skeletal muscle atrophy.

Abbreviations

AChE: acetylcholinesterase; BYHWT: Buyang Huanwu Tang; cDNA: complementary DNA; DSMA: denervated-dependent skeletal muscle atrophy; HE: hematoxylin and eosin; PBS: phosphate-buffered saline; qRT-PCR: quantitative RT-PCR; RIPA: radioimmunoprecipitation assay; SMA: skeletal muscle atrophy.

Author contributions

XYM and JC designed the present paper. LZ, YFH, and HX performed experiments or tests. YFH made statistical analysis. HX conducted the literature review. LZ wrote the manuscript. XYM and JC made a critical revision of this manuscript.

Ethics approval and consent to participate

All of the tests or experiments were conducted based on the Guidelines of Institutional Animal Care. The research was approved by the Ethics Committee of Traditional Chinese Medicine in Nanjing University.

Acknowledgment

This research was funded by the National Natural Science Foundation of PRC (Grant No: 81302890), Natural Science Foundation of Colleges and Universities in Jiangsu Province (Grant No: 13KJB360003), Natural Science Foundation of Jiangsu Province (Grant No: BK2011816), Natural Science Foundation (Grant No: 20123237120004) and Jiangsu Overseas Visiting Scholar Program for University Prominent Young & Middle-aged Teachers and Presidents.

Conflict of Interest

The authors declare no competing financial or commercial interests in this manuscript.

Submitted: October 30, 2019
Accepted: February 07, 2020
Published: March 30, 2020

References

Chen, D. Q., Zheng, X. D., Cao, Y., He, X. D., Nian, W. Q., Zeng, X. H. and Liu, X. Y. (2017) Long non-coding RNA LINC00628 suppresses the growth and metastasis and promotes cell apoptosis in breast cancer. *European Review for Medical and Pharmacological Science* **21**, 275-283.

Cheng, C., Li, P., Wang, Y. G., Bi, M. H. and Wu, P. S. (2016) Study on the expression of VEGF and HIF-1alpha in infarct area of rats with AMI. *European Review for Medical and Pharmacological Science* **20**, 115-119.

Du, Y., Ge, Y., Xu, Z., An, N., Gu, X., Meng, H., Lin, Z., Zhu, D., Shi, J., Zhuang, R., Wu, X., Wang, X. and Yang, Z. (2018) Hypoxia-inducible factor 1 alpha (HIF-alpha)/vascular endothelial growth factor (VEGF) pathway participates in angiogenesis of myocardial infarction in muscone-treated mice: preliminary study. *Medical Science Monitor* **24**, 8870-8877.

Hsieh, C. H., Jeng, S. F., Wu, C. J., Lu, T. H., Yang, J. C., Chen, Y. C., Lin, C. J. and Rau, C. S. (2011) Altered expression of the microRNAS and their potential target genes in the soleus muscle after peripheral denervation and reinnervation in rats. *Journal of Trauma* **70**, 472-480.

Huang, Q. K., Qiao, H. Y., Fu, M. H., Li, G., Li, W. B., Chen, Z., Wei, J. and Liang, B. S. (2016) MiR-206 attenuates denervation-induced skeletal muscle atrophy in rats through regulation of satellite cell dif-

ferentiation via TGF-beta 1, Smad3, and HDAC4 signaling. *Medical Science Monitor* **22**, 1161-1170.

Law, N. C., Weck, J., Kyriss, B., Nilson, J. H. and Hunzicker-Dunn, M. (2013) Lhctr expression in granulosa cells: roles for PKA-phosphorylated beta-catenin, TCF3 and FOXO1. *Molecular Endocrinology* **27**, 1295-1310.

Li, G., Li, Q. S., Li, W. B., Wei, J., Chang, W. K., Chen, Z., Qiao, H. Y., Jia, Y. W., Tian, J. H. and Liang, B. S. (2016) miRNA targeted signaling pathway in the early stage of denervated fast and slow muscle atrophy. *Neural Regeneration Research* **11**, 1293-1303.

Liu, C., Zhou, L. and Shui, Z. (2003) Tongqiao huoxue tang and buyang huanwu tang for treatment of vascular dementia-a report of 36 cases. *Journal of Traditional Chinese Medicine* **23**, 243-245.

Livak, K. J. and Schmittgen, T. D. (2001) Analysis of relative gene expression data using real-time quantitative PCR and the 2(-Delta Delta C(T)) method. *Methods* **25**, 402-408.

Nagpal, P., Plant, P. J., Correa, J., Bain, A., Takeda, H., Rotin, D., Bain, J. R. and Batt, J. A. (2012) The ubiquitin ligase Nedd4-1 participates in denervation-induced skeletal muscle atrophy in mice. *PLoS One* **7**, e46427.

Nakata, T., Ito, M., Azuma, Y., Otsuka, K., Noguchi, Y., Okumura, A., Shiraishi, K., Masuda, A., Natsume, J., Kojima, S. and Ohno, K. (2013) Mutations in the C-terminal domain of CoIQ in endplate acetylcholinesterase deficiency. *Human Mutation* **34**, 997-1004.

Romeo-Guitart, D., Fores, J., Navarro, X. and Casas, C. (2017) Boosted regeneration and reduced denervated muscle atrophy by neurol-heal in a pre-clinical model of lumbar root avulsioin with delayed reimplantation. *Science Report* **7**, 12028.

Rom, O. and Reznick, A. Z. (2016) The role of E3 ubiquitin-ligases MuRF-1 and MAFBX in loss of skeletal muscle mass. *Free Radical Biology and Medicine* **98**, 218-230.

Rrey, S. P., Jansen, H., Raschke, M. J., Meffert, R. H. and Ochman, S. (2012) VEGF improves skeletal muscle regeneration after acute trauma and reconstruction of the limb in a rabbit model. *Clinical Orthopaedics and Related Research* **470**, 3607-3614.

Tajrishi, M. M., Shin, J., Hetman, M. and Kumar, A. (2014) DNA methyltransferase 3a and mitogen-activated protein kinase signaling regulate the expression of fibroblast growth factor-inducible 14 (Fn14) during denervation-induced skeletal muscle atrophy. *Journal of Biological Chemistry* **289**, 19985-19999.

Tamura, Y., Kitaoka, Y., Matsunaga, Y., Hoshino, D. and Hatta, H. (2015) Daily heart stress treatment rescues denervation-activated mitochondrial clearance and atrophy in skeletal muscle. *Journal of Physiology* **593**, 2707-2720.

Tang, Y. H., Li, H. and Chen, B. Y. (2006) Effect of active fraction of buyang huanwu detection on caspase expression in rats after focal cerebral ischemic reperfusion. *Zhongguo Zhong Xi Yi Jie He Za Zhi* **26**, 533-537. (In Chinese)

Tian, J. S., Zhai, Q. J., Zhao, Y., Chen, R. and Zhao, L. D. (2017). 2-(2-benzofuranyl)-2-imidazoline (2-BFI) improved the impairments in AD rat models by inhibiting oxidative stress, inflammation and apoptosis. *Journal of Integrative Neuroscience* **16**, 385-400.

Wei, R. L., Teng, H. J., Yin, B., Xu, Y., Du, Y., He, F. P., Chu, K. T., Luo, B. Y. and Zheng, G. Q. (2013) A systematic review and meta-analysis of buyang huanwu decoction in animal model of focal cerebral ischemia. *Evidence-Based Complementary and Alternative Medicine* **2013**, 138484.

Xiang, Y., Li, S., Liu, X., Li, J., Sun, Q., Chen, Y., Du, Y. and Wu, J. (2019) Neuroacanthobytosis: a case report of chorea-acanthocytosis. *Journal of Integrative Neuroscience* **18**, 197-201.

Zanella, S., Buccelletti, F., Franceschi, F., Vassiliadis, A., Ramponi, C., Sivolella, S., Zanoni, A. and Lumachi, F. (2018) Transnasal sphenopalatine ganglion blockade for acute facial pain: a prospective ransomized case-control study. *European Review for Medical and Pharmacological Science* **22**, 210-216.

Zhang, X., Mu, L., Su, H. and Sobotka, S. (2011) Locations of the motor endplate band and motoneurons innervating the sternomastoid muscle in the rat. *Anatomical Record (Hoboken)* **294**, 295-304.

Zhang, Y. K., Han, X. Y. and Che, Z. Y. (2010) Effects of Buyang Huanwu Tang combined with bone marrow mesenchymal stem cell transplantation on the expression of VEGF and Ki-67 in the brain tissue of the cerebral ischemia-reperfusion model rat. *Journal of Traditional Chinese Medicine* **30**, 278-282.

Zhao, Y. T., Yan, J. Y., Han, X. C., Niu, F. L., Zhang, J. H. and Hu, W. N. (2017) Anti-proliferative effect of digoxin on breast cancer cells via inducing apoptosis. *European Review for Medical and Pharmacological Science* **21**, 5837-5842.

Zhou, L., Huang, Y., Xie, H. and Mei, X. (2018) Buyang Huanwu Tang improves denervation-dependent muscle atrophy by increasing ANGPTL4 and increases NF-kB and MURF1 levels. *Molecular Medicine Reports* **17**, 3674-3680.

Zhou, L., Huang, Y. F., Xie, H., Mei, X. Y. and Gao, J. (2019) Buyang Huanwu Tang alleviates inflammation and improves motor endplate functions in DSMA rat models by activating several biological molecules and associated signaling pathways. *American Journal of Translational Research* **11**, 3056-3068.

Zhou, L., Mei, X. Y., Wu, H. X., Xie, H., Tang, X. M. and Sun, H. L. (2011) Experimental study on Buyang Huanwu decoction (Chinese characters: see text) for promoting functional recovery of crushed common peroneal nerve in rats. *Zhongguo Gu Shang* **24**, 249-252. (In Chinese)

Zuo, H., Lin, T., Wang, D., Peng, R., Wang, S., Gao, Y., Xu, X., Zhao, L., Wang, S. and Su, Z. (2015) RKIP regulates neural cell apoptosis induced by exposure to microwave radiation party through the MEK/ERK/CREB pathway. *Molecular Neurobiology* **51**, 1520-1529.